Design and Evaluation of an Active Antenna for a 29–47 MHz Radio Telescope Array

S.W. Ellingson, *Senior Member, IEEE*, J.H. Simonetti, and C.D. Patterson *Senior Member, IEEE*

***Abstract*— The Eight-meter-wavelength Transient Array (ETA) is a new radio telescope consisting of 12 dual-polarized, 38 MHz-resonant dipole elements which are individually instrumented, digitized, and analyzed in an attempt to detect rare and as-yet undetected single dispersed pulses believed to be associated with certain types of astronomical explosions. This paper presents the design and demonstrated performance of ETA's dipole antennas. A inverted V-shaped design combined with a simple and inexpensive active balun yields sensitivity which is limited only by the external noise generated by the ubiquitous Galactic synchrotron emission over a range greater than the 27–49 MHz design range. The results confirm findings from a recent theoretical analysis [1], and the techniques described here may have applications in other problems requiring *in situ* evaluation of large low-frequency antennas.**

***Index Terms*— Radio astronomy, active antenna**

I. Introduction

The Eight-meter-wavelength Transient Array (ETA) is a new radio telescope designed to observe a variety of postulated but as-yet undetected astrophysical phenomena which are suspected to produce single pulses detectable at relatively long wavelengths. Potential sources for such pulses include the prompt emission associated with gamma ray bursts and the self-annihilation of primordial black holes. Although such sources may be potentially quite strong by astronomical standards, they are difficult to detect using existing telescopes due to their transient and unpredictable nature. ETA, in contrast, is designed to provide roughly uniform (albeit very modest) sensitivity over most of the visible sky, all the time. The complete array consists of 12 dual-polarized dipole-like elements (i.e., 24 radio frequency inputs) at the Pisgah Astronomical Research Institute (PARI), located in a rural mountainous region of Western North Carolina ($35^\circ\ 11.98'$ N, $82^\circ\ 52.28'$ W). Each dipole is individually instrumented and digitized. The digital signals are combined to form fixed "patrol beams" which cover the sky, and the output of each beam is searched for the unique time-frequency signature expected from short pulses which have been dispersed by the ionized interstellar medium. Additional information about ETA and its science objectives are available at the project web site [3].

ETA is designed to operate in the range 29–47 MHz, which is a response to a number of factors. First, some astrophysical theories suggest the possibility of strong emission by the sources of interest in the HF and lower VHF bands, limited at the low end by the increasing

This work was supported by the National Science Foundation under Grant No. AST-0504677, and by the Pisgah Astronomical Research Institute. This is an expanded version of a conference paper [2].

Bradley Dept. of Electrical and Computer Engineering, Virginia Polytechnic Institute and State University, Blacksburg, VA; ellingson@vt.edu.

opacity of the ionosphere to wavelengths longer than about 20 m (15 MHz). Useable spectrum is further limited by the presence of strong interfering man-made signals below about 30 MHz (e.g., international shortwave broadcasting and Citizen's Band (CB) radio) and above about 50 MHz (e.g., broadcast television), which make it difficult to observe productively outside this range. This amounts to 25% bandwidth and thus a thin dipole would ordinarily not be suitable. At these frequencies, however, the ubiquitous Galactic synchrotron emission is extraordinarily strong and can easily be the dominant source of noise in the observation. From previous work [1], it is known that a simple dipole-like antenna, used in conjunction with a preamplifier having a modest noise temperature, may exhibit nearly the best possible sensitivity even when impedance matching is very poor, because external Galactic noise, as opposed to internally-generated amplifier noise, may constrain the signal-to-noise ratio (SNR) which can be achieved at the preamplifier output. This concept is also being employed in the new radio telescope LOFAR [4], now being planned for construction in Northern Europe, although technical and performance details are not publicly available. In this paper, we describe the design of the antenna and preamplifier for ETA, and report the results of an *in situ* measurement of one of the installed elements. It is shown that the design yields sensitivity which is in fact limited primarily by Galactic noise over the desired frequency range. Furthermore, the results demonstrate good agreement with estimates obtained using the theoretical analysis presented in [1].

This paper is organized as follows. Section II describes the design of the ETA active antenna. Section III describes the methodology used to collect and reduce data obtained from *in situ* testing of the antenna. Section IV presents the results of measurements demonstrating Galactic noise-limited operation. Conclusions are summarized in Section V.

Fig. 1. The 10-element core array of ETA. The antenna under test is in the center. The remaining 9 antenna stands form a circle of radius 8 m.

II. The ETA Active Antenna

Figure 1 shows the central "core array" of ETA, where most of the antennas are located. The antennas are installed as "stands," where each stand is a mast supporting two orthogonally-polarized dipole-like elements, with one dipole oriented along a north-south axis and the other oriented along an east-west axis. The antenna under test in this case is the North-South oriented dipole in the center of the array, shown in Figure 2. The dipole arms are constructed from $\frac{3}{4}$-in (1.9 cm) $\times$ $\frac{3}{4}$-in aluminum angle (i.e., "L"-shaped) stock, $\frac{1}{8}$-in (~ 3 mm) thick. This material was chosen as a tradeoff between ease of construction (favoring thinner dimensions) and bandwidth (favoring thicker dimensions). Alternatives considered included stranded copper wire (diameter ~ 1.5 mm), which is very easy to work with but yields insufficient impedance bandwidth to cover the range 29–47 MHz; and $\frac{3}{4}$-in wide $\times$ $\frac{1}{8}$-in thick aluminum strip stock, which yielded acceptable bandwidth but lacked sufficient rigidity. Angle stock, in contrast, is quite rigid and exhibits slightly greater bandwidth than strip stock. The tips of each dipole are stabilized using nylon rope which is staked to the ground; this is primarily to prevent damage due to high wind speeds.

The dipole dimensions are shown in Figure 3. The total length of a dipole (including both arms and feed

Fig. 2. The ETA antenna stand under test, showing dipole arms and feed region in greater detail.

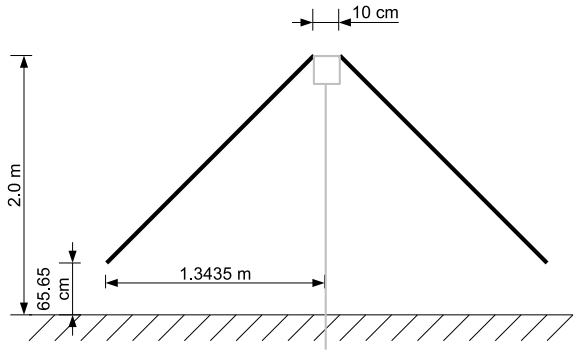

Fig. 3. Key dimensions of the dipole.

gap) is 3.8 m, which was selected to make the dipole resonant at approximately 38 MHz, which is the center of the frequency range of interest. The dipole arms are bent down at an angle of 45° to broaden the pattern. Although the pattern is of interest in this application, this is quite difficult to measure due to the large size of the antenna and its complex interaction with the ground. Predictions of the pattern for this geometry, obtained from moment method calculations, are presented in [1]. As one might expect, the pattern has maximum at zenith and null along the horizon, with little variation between E- and H-planes and some variation over the design frequency range.

The antenna terminals are located at the top of a mast 2-m in height, corresponding to approximately one-quarter wavelength above the ground at resonance. The mast is constructed from PVC electrical conduit of diameter 4-in (10 cm).

Each dipole is connected to a preamplifier located inside the mast, separated from the dipole by an ABS plastic end cap as shown in Figure 4. The interior construction of the preamplifier is shown in Figure 5. The preamplifier is a custom design adapted from previous work [5]. The design consists of two Mini-Circuits GALI-74 monolithic microwave integrated circuit (MMIC) amplifiers [6] arranged as a differential pair, with one dipole arm attached to each amplifier. Each GALI-74 has an input impedance of 50Ω, thus the preamplifier presents an input impedance of 100Ω to the dipole. Each MMIC is powered using a 9 VDC supply which is current-limited using a 56Ω bias resistor. The amplifier outputs are combined through a Mini-Circuits ADT2-1T-1P surface-mount transformer [7], configured as a balun. The single-ended output of the transformer is output to coaxial cable through a Type-N connector. Additional details, including schematics and circuit board layout files, are available at [3]. This design yields 23.25 ± 0.15 dB gain over the range 29–47 MHz, as determined by measurement. The noise temperature of the preamplifier is estimated to be roughly 300 K, which has not been measured directly but is consistent with the findings presented later in this paper.

The 100Ω input impedance of the preamplifier does not yield the optimal impedance match over the design range; in fact, a higher impedance could significantly improve the quality of the match above 38 MHz [1]. However, it is demonstrated in Section IV that the sensitivity of this design is strongly dominated by external (Galactic) noise; thus, any additional improvement in the match would not significantly improve sensitivity.

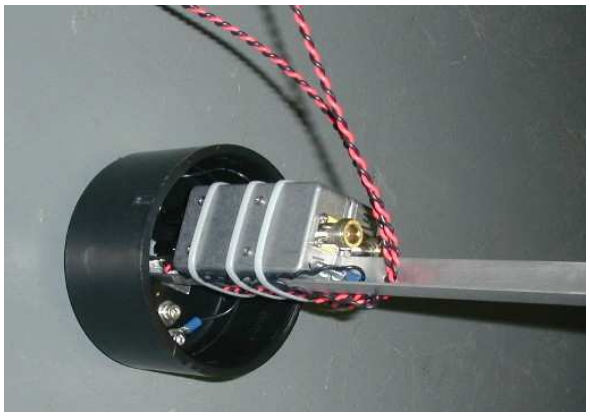

Fig. 4. Mast end cap removed to show mounting of preamplifiers and connection to dipoles.

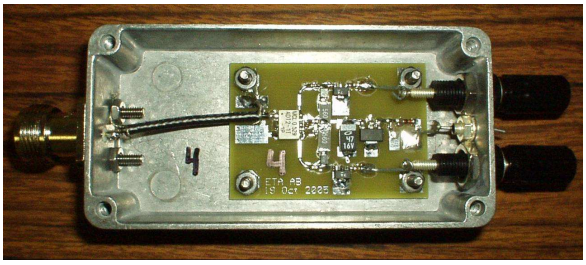

Fig. 5. Cover removed from a preamplifier to show circuit board and connections to dipole (right) and coaxial cable (left).

Furthermore, to increase the input impedance of this design would necessitate the use of additional passive components between the dipole and the MMIC amplifiers, which would certainly increase the noise figure as well as the overall complexity and cost.

As there is no filter present between the dipole and the preamplifier, an important practical consideration is the linearity of the preamplifier. The input-referred 1-dB compression point of this design has determined by measurement to be -3 dBm, which seems to be sufficiently linear to avoid detectible intermodulation under the RFI conditions present at the ETA site.

Components in the signal path which are not part of the active antenna but are relevant to its measurement and analysis are as follows. The output of the preamplifier is connected to RG-58 (50Ω) coaxial cable. For the antenna under test in this paper, the cable is 32 m in length and introduces 3.2 dB loss at 38 MHz with a frequency dependence proportional to $\nu^{-0.5}$, where ν is frequency. The signal passes through a PolyPhaser Model IS-B50LN-C0 lightning protector, which has VSWR better than 1.1:1 and insertion loss < 0.1 dB over the frequency range of interest, and thus has negligible effect. The signal is then processed through an analog receiver of custom design which amplifies and filters the signal (no mixing or tuning). The analog receiver provides 52.2 dB gain at 38 MHz, and is -1.2 dB and -1.8 dB down at 29 MHz and 47 MHz respectively, all determined by measurement. It is the analog receiver that provides frequency selectivity; the preamplifier response in contrast is essentially flat from 10 MHz to 80 MHz.

III. Methodology

The main objective of this evaluation is to confirm that the sensitivity of the dipole-preamplifier combination is strongly limited by the irreducible noise associated with the Galactic synchrotron emission, as opposed to any internal or terrestrial noise mechanism. The strategy shall be to measure the power spectrum at the output of the analog receiver, remove the frequency responses (including gain) of all components, and then compare the result to separate, well-established values for the Galactic background.

Measurement and removal of the frequency response is straightforward for all components except for the antenna itself. The size and method of installation of the antenna make it quite difficult to measure accurately *in situ*. For the purposes of this testing, however, the antenna can be conveniently characterized using the methodology described in [1]. In this approach, the

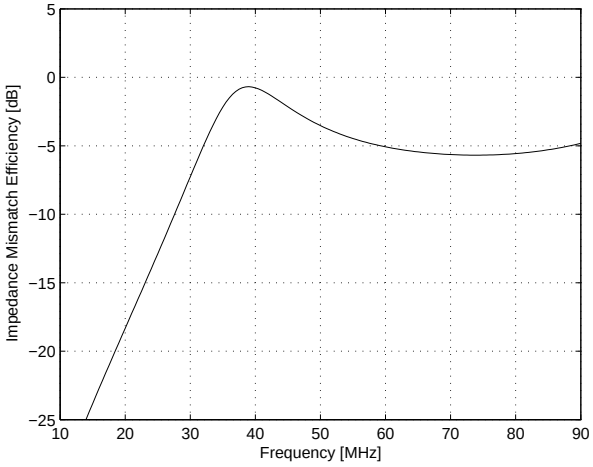

Fig. 6. Impedance mismatch efficiency (IME) of an ETA dipole connected to a 100Ω active balun input impedance.

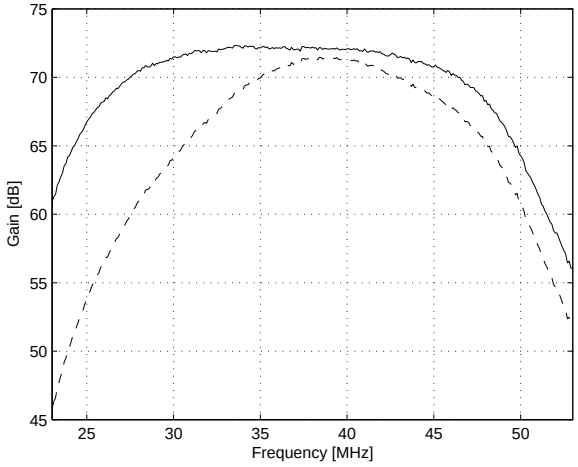

Fig. 7. *Solid/Top*: The transfer function including the active balun, coax, and analog receiver. *Broken/Bottom*: Same, except now including the antenna response (IME).

antenna is described in terms of its impedance mismatch efficiency (IME), which is defined as $1 - |\Gamma|^2$ where Γ is the reflection coefficient at the interface between the dipole and (in this case) the 100Ω active balun input impedance. In effect, IME is the fraction of the antenna temperature T_{sky} that is effectively delivered to the active balun. IME in this case was determined using calculations of the antenna terminal impedance obtained from NEC-2 moment method software, in which the dipole arms were modeled as aluminum wires of circular cross section having diameter equal to the width of the angle stock (1.9 cm). In these calculations, the ground is included and is assumed to have conductivity $\sigma = 5 \times 10^{-3}$ S/m and relative permittivity $\epsilon_r = 13$. The resulting IME shown in Figure 6.

The transfer function including only the active balun, coaxial cable, and analog receiver is shown in Figure 7. The same result including IME is also shown. The latter is the expected total transfer function from antenna temperature (nominally dominated by Galactic noise) to the output of the analog receiver.

The output of the analog receiver was captured using a spectrum analyzer interfaced to a laptop PC, which provided automated control and data archiving. To ensure linear and unbiased measurement of the noise spectrum, the spectrum analyzer was configured to use "sample" mode detection, as opposed to "quasi-peak" detection mode (the default mode for most spectrum analyzers). Removal of the instrumental responses described above yield an estimate of the power spectral density S_{sky} at the antenna terminals under matched load conditions. This is converted to antenna temperature via the relationship $S_{sky} = e_r k T_{sky} \Delta\nu$, where k is Boltzmann's constant (1.38×10^{-23} J/K), $\Delta\nu$ is the resolution bandwidth of the spectrum analyzer, and e_r is the loss due to the finite conductivity of the materials used to make the antenna, and absorption by the imperfect (nonperfectly-conducting) ground. The former is negligible in this case, whereas the latter is shown in [1] to be between 2.5 dB and 3.9 dB over the range 30–90 MHz (increasing with increasing frequency) for the ground conditions assumed in the antenna impedance calculation.

As explained in [1], the expected value of T_{sky} is

approximately the same for any antenna having a roughly hemispherical pattern, and is given by

$$T_{sky} = \frac{1}{2k} I_\nu \frac{c^2}{\nu^2} \ , \tag{1}$$

where c is the speed of light and I_ν is intensity, which has units of W m^{-2} Hz^{-1} sr^{-1}. From observations of the Galactic polar region by Cane [8] as explained in the appendix of [1], we shall assume

$$I_\nu = I_g \ \nu_{\rm MHz}^{-0.52} + I_{eg} \ \nu_{\rm MHz}^{-0.80} \ , \tag{2}$$

where $I_g = 2.48 \times 10^{-20}$, $I_{eg} = 1.06 \times 10^{-20}$, and $\nu_{\rm MHz}$ is frequency in MHz. The resulting value of T_{sky} decreases monotonically from $\sim 11,000$ K at 29 MHz to $\sim 5,000$ K at 47 MHz. The general strategy shall be to compare this model for the antenna temperature of an earth-bound low-gain antenna to the derived antenna temperature starting from the spectrum analyzer measurements and removing the instrumental responses. If the agreement is sufficiently good, we can assume that the preamplifier noise temperature is sufficiently low such that the preamplifier output is strongly Galactic noise-dominated.

IV. Results

We measured the power spectral density at the output of the analog receiver continuously for approximately 2 days beginning at about 8:00 am EDT on August 2, 2006. Figure 8 shows the output of the analog receiver integrated (averaged) over the entire observation time. The similarity to the "with IME" curve in Figure 7 is apparent, although the measurement includes the frequency dependence of the Galactic background, as we shall soon see. Also apparent in Figure 8 is strong RFI above 50 MHz (TV stations); note these have been suppressed by at least 50 dB by the analog receiver, but pass through the active balun at nearly full strength.

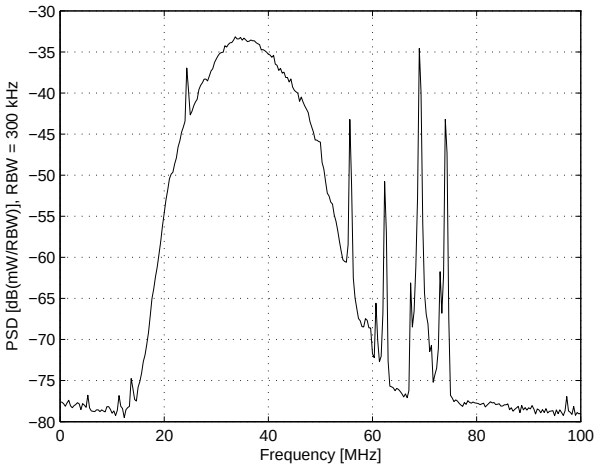

Fig. 8. Output of the analog receiver: Integrated (i.e., mean) power spectral density after 2 days of continuous measurement. No attempt has been made to calibrate the frequency response. Strong signals above 50 MHz are analog TV stations. The noise floor at about -78 dB is due to the spectrum analyzer.

Figure 9 shows the same data, but now calibrated to remove the analog receiver, coaxial cable, active balun, and antenna IME. Thus, this represents power actually incident on the antenna. Clearly visible is a log-linear slope in the noise floor which, as we shall see below, is attributable to the Galactic background. The noise floor exhibits a slow ripple of about 0.5 dB towards the edges of the passband which is believed to be due to a subtle impedance mismatch between the output of the active balun and the long coax cable. Also, some of the signals which interfere with ETA observations are apparent, including activity around 27 MHz (a combination of HF and CB communications), an intermittently strong narrowband signal at 42.6 MHz (known to be a nearby base station operated by the local state police), and various (mostly unidentified) interference between 46 MHz and 49 MHz. The peak at 50 MHz is due to beacon (broadcast) signals in the 6-meter amateur radio band.

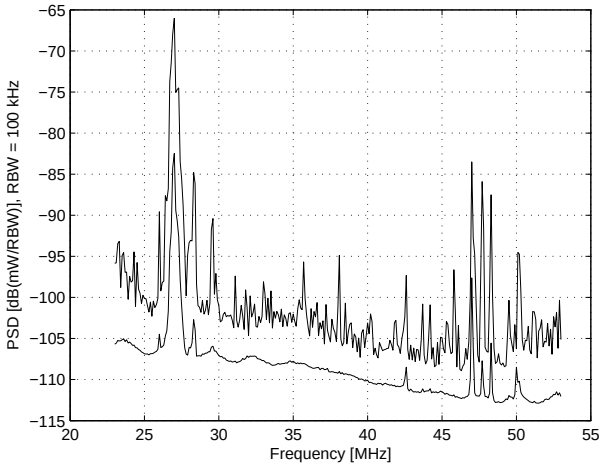

Fig. 9. Output of the analog receiver, summarizing 2 days of continuous observations, with transfer functions of the analog receiver, coaxial cable, active balun, and antenna (IME) removed. *Top:* Maximum value ever observed, *Bottom:* Mean.

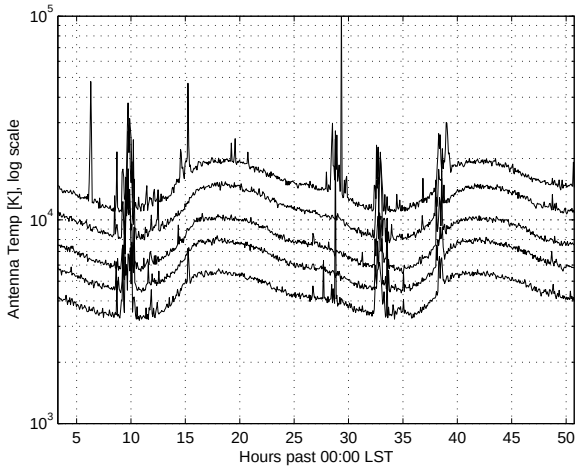

Fig. 10. Total power in a 1 MHz bandwidth, after removal of all instrumental transfer functions, including antenna IME. Center frequencies are, top to bottom: 29.5, 34.5, 39.0, 41.5, and 46.0 MHz.

Figure 10 shows the total power in a 1 MHz bandwidth at 5 frequencies spread across the band of interest, after removal of all instrumental responses including antenna IME. Results are now expressed in terms of antenna temperature. A diurnal variation is clearly visible, and is attributable to the non-uniform distribution of the Galactic noise intensity over the sky. The resulting antenna temperature is greatest when the plane of the Galaxy (including the relatively bright Galactic center) is high in the sky, and lowest when the polar region of the Galaxy is high in the sky. The diurnal variation appears to be the same at all frequencies with no evidence of flattening around the daily minimums, which suggests the noise being measured is strongly dominated by this mechanism.

Also apparent in Figure 10 are bursts of interference at 10 hours and 33 hours past 00:00 local sidereal time (LST), which are of unknown origin but believed to be locally-generated. Another set of interference bursts occurring 16 hours and 29 hours past 00:00 LST are actually temporary enhancements of long-distance communications due to transient ionospheric "sporadic E" conditions. Most of the time, however, each of these bands contain no detectible signals.

It is possible to anticipate the diurnal variation observed in Figure 10 using data extrapolated from existing astronomical surveys and thereby obtain independent confirmation that the results are consistent with Galactic noise-limited operation. Rogers, Pratap, and Kratzenberg (2004) [9] demonstrated that the 408 MHz sky survey of Haslam *et al.* (1982) [10] could be extrapolated to 327 MHz and used for this purpose simply by scaling the survey temperatures by the factor $(\nu/(408\text{ MHz}))^{-2.55}$. Figure 11 shows the 39 MHz result from Figure 10 with a prediction obtained by convolving the 408 MHz survey data with a simple model for the ETA antenna pattern, scaling the result by $((39\text{ MHz})/(408\text{ MHz}))^{-2.55}$, and then dividing by 2 (3 dB) to account for ground loss. Note that the agreement is quite reasonable despite the long reach of the extrapolation and the potential for error in the antenna pattern and ground loss estimates.

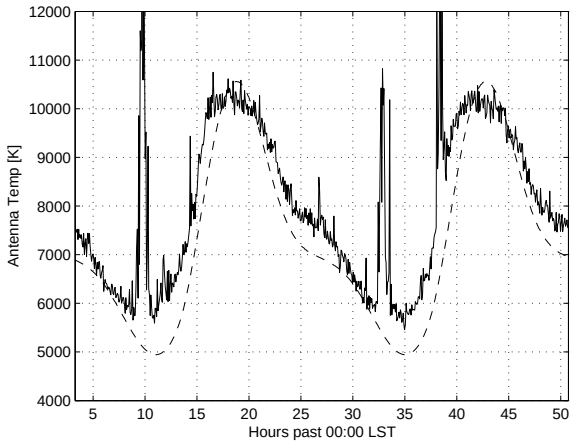

Fig. 11. 39.0 MHz result from Figure 10 (*solid*) shown with result predicted by extrapolation from 408 MHz sky survey (*dashed*).

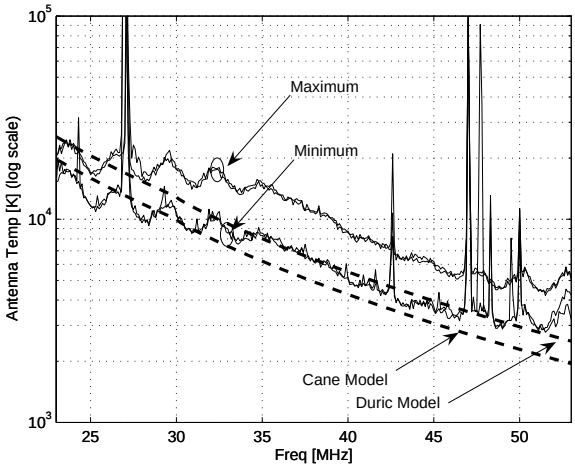

Fig. 12. Frequency dependence of integrated spectrum. The thick dashed curves are predicted values of the Galactic background, including ground loss. The "maximum" curves are the integrated spectrum from two separate 1 h observations spaced 24 h apart, taken at times corresponding to maximum antenna temperature. The "minimum" curves are integrated spectrum from two separate 1 h observations spaced 24 h apart, taken at times corresponding to minimum antenna temperature.

Figure 12 shows spectra obtained by averaging over about 1 hour of observations (note that effective integration time is actually much less than this due to the use of a spectrum analyzer). Peaks around 27 MHz, 42.6 MHz, 47–49 MHz, and 50 MHz are interference, as previously explained. The four spectra shown correspond to observations beginning 11:30 LST (a daily minimum), 19:00 LST (a daily maximum), and the same two times 24 hours later. Also shown is a prediction of the spectrum of the Galactic background based on the simple static sky model described in the previous section, and assuming 3 dB ground loss. Note that the measurements agree reasonably well with the static sky models. The fact that the Cane model result is close to the "minimum" result can be attributed to the fact that the Cane model is specific to the Galactic polar regions and is not applicable to the Galactic equatorial region (including the Galactic Center), which is partially visible from the observing site and significantly brighter. A modification by Duric [11] based on the work of Tokarev [12] (also explained in the appendix of [1]) increases I_g to 3.2×10^{-20} to account for this. This modification yields a result (also shown in Figure 12) which is very close to the "minimum" observation. The dominant remaining error is probably due to the simple antenna model implicit in Equation 1.

Finally, note that measurements taken 24 h apart are in very close agreement (within 0.05 dB (1%) at 38 MHz), which demonstrates the repeatability of the measurement. We conclude that the sensitivity of this active antenna is strongly Galactic noise limited over both time of day and frequency, at least in the design range 29-47 MHz.

It is tempting to try to estimate the noise temperature of the preamplifier based on the above data, but in practice this is difficult to do accurately. It is obvious from the above data that the preamplifier noise temperature is much less than 4000 K. If we assume this means that it is at least 10 dB less, then the preamplifier noise temperature is upper bounded at 400 K. The actual noise

temperature is believed to be less than 300 K, but any value less than 1000 K or so will probably yield results similar to those shown here.

V. Conclusions

This paper has presented the design of an active antenna for a radio telescope array operating in the range 29–47 MHz. It has been demonstrated by measurement over a two-day period that the sensitivity of this antenna is limited by irreducible natural noise associated with Galactic synchrotron emission, and in this sense exhibits the best possible performance over the frequency range of interest. Thus, additional efforts to optimize the active antenna – e.g., to improve impedance bandwidth or reduce noise temperature – are unlikely to yield significant benefits in this application. It is worth noting that the procedure used to evaluate this antenna might also have application in the measurement of other low-frequency antennas, which similarly are difficult to measure due to their size or the need to make measurements *in situ*.

Acknowledgments

The authors acknowledge helpful discussions pertaining to the design of the preamplifier with B. Hicks of the U.S. Naval Research Laboratory. Students S. Cutchin, A. Lee, and C. Magruder, all of Virginia Tech, participated in assembling and installing the equipment described in this paper. PARI constructed the antenna masts and coaxial cable system described in this paper.

References

[1] S.W. Ellingson, "Antennas for the Next Generation of Low Frequency Radio Telescopes," *IEEE Trans. Ant. & Prop.*, Vol. 53, No. 8, August 2005, pp. 2480-9.

[2] S.W. Ellingson, C.D. Patterson, J.H. Simonetti, "Design and Demonstration of an Antenna for a New 29–47 MHz Radio Telescope Array," *2006 IEEE Int'l Ant. & Prop. Symp.*, Albuquerque, NM, July 2006.

[3] ETA Project Website, http://www.ece.vt.edu/swe/eta.

[4] H. R. Butcher, "LOFAR: First of a new generation of radio telescopes," in *Proc. SPIE*, vol. 5489, Sep. 2004, pp. 537–44. See also web site http://www.lofar.org.

[5] B. Hicks, U.S. Naval Research Laboratory, personal communication.

[6] Mini-Circuits Corp., "Surface Mount Monolithic Amplifier GALI-74" (datasheet), Rev. B, 2005.

[7] Mini-Circuits Corp., "Surface Mount RF Transformer ADT2-1T-1P" (datasheet), Rev. B, 2005.

[8] H. V. Cane, "Spectra of the nonthermal radio radiation from the galactic polar regions," *Monthly Notice Royal Astronomical Society*, vol. 189, p. 465, 1979.

[9] A.E.E. Rogers, P. Pratap, and E. Kratzenberg, "Calibration of Active Antenna Arrays using a Sky Brightness Model," *Radio Sci.*, Vol. 39, RS2023, 2004.

[10] C.G.T. Haslam *et al.*, "A 408 MHz All-Sky Continuum Survey. II. The Atlas of Contour Maps," *Astron. Astrophys. Suppl. Ser.*, Vol. 47, January 1982, pp. 1–143.

[11] Duric, N. *et al.*, "RFI Report for the U.S. South-West," LOFAR project report, 2003, available at http://www.haystack.mit.edu/ast/arrays/mwa/site/rfi_download.html.

[12] Tokarev, Y., "Cosmic Background with Model of Cloudy Interstellar Medium," *VIII Russian-Finnish Sym. on Radioastronomy*, St. Petersburg, Russia, 1999, available at http://www.gao.spb.ru/english/publ-s/viii-rfs/.

PLACE PHOTO HERE

Steven W. Ellingson (S'87-M'90-SM'03) received the B.S. degree in electrical and computer engineering from Clarkson University, Potsdam, NY, in 1987, and the M.S. and Ph.D. degrees in electrical engineering from the Ohio State University, Columbus, in 1989 and 2000, respectively. From 1989 to 1993, he served on active duty with the U.S. Army. From 1993 to 1995, he was a Senior Consultant with Booz-Allen and Hamilton, McLean, VA. From 1995 to 1997, he was a Senior Systems Engineer with Raytheon E-Systems, Falls Church, VA. From 1997 to 2003, he was a Research Scientist with the Ohio State University ElectroScience Laboratory. Since 2003 he has been an Assistant Professor in the Bradley Department of Electrical & Computer Engineering at Virginia Polytechnic Institute & State University. His research interests include antennas & propagation, applied signal processing, and instrumentation.

PLACE
PHOTO
HERE

John H. Simonetti received the B.S. degree from SUNY Stony Brook in Physics in 1978 and the M.S. and Ph.D. degrees in Astronomy and Space Sciences from Cornell University in 1982 and 1985 respectively. He is an Associate Professor in the Department of Physics at Virginia Polytechnic Institute & State University.

PLACE
PHOTO
HERE

Cameron D. Patterson (M'99-SM'05) received the B.S. and M.S. degrees in computer science from the University of Manitoba, Canada, in 1980 and 1983 respectively, and the Ph.D. degree in computer science from the University of Calgary, Canada, in 1992. From 1992 to 1994, he held an NSERC Industrial Research Fellowship at the Alberta Microelectronic Centre. From 1994 to 2003 he was a senior researcher at Xilinx, the leading manufacturer of Field-programmable Gate Arrays. Since 2003 he has been an Associate Professor in the Bradley Department of Electrical & Computer Engineering at Virginia Polytechnic Institute & State University. His research interests include reconfigurable and secure computing, electronic design automation, and computational number theory.

LIST OF FIGURES